Inorganic Chemistry

Article

pubs.acs.org/IC

Synthesis and Analysis of a Family of Cerium(IV) Halide and Pseudohalide Compounds

Ursula J. Williams, Patrick J. Carroll, and Eric J. Schelter*

P. Roy and Diana T. Vagelos Laboratories, Department of Chemistry, University of Pennsylvania, 231 South 34th Street, Philadelphia, Pennsylvania 19104, United States

Supporting Information

ABSTRACT: The first complete series of isostructural cerium(IV) halide complexes in a conserved ligand framework was isolated by halogen-exchange reactions of $CeF[N(SiMe_3)_2]_3$ with Me_3SiX (X = Cl^-, Br^-, I^-). The use of Me_3SiX reagents represents a useful method for obtaining cerium(IV) complexes. Spectroscopic, electrochemical, and computational analyses were used to describe the effects of halide coordination on the cerium(IV) metal center. Cerium(IV) complexes of the pseudohalide ligands: N_3^- and NCS^- were also synthesized and evaluated in comparison to the halide congeners. The results showed that the complexes exhibited reduction potentials and electronic absorption energies that varied with the identity of the halide or pseudohalide ligand.

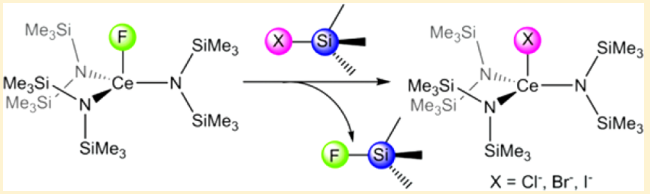

INTRODUCTION

Few studies have systematically considered the effects of ligands on the properties of the cerium ion in its tetravalent oxidation state. One of the simplest families of ligands to consider is the halides, which are well explored in cerium(III) chemistry and lanthanide chemistry in general but which are much less developed in cerium(IV) chemistry. In the materials chemistry of cerium(IV), the binary halides are unstable in all cases except for the fluoride, CeF_4.[1] In molecular chemistry, cerium(IV) chloride complexes have been isolated using a variety of ancillary ligand platforms.[2−6] Other reported examples of molecular cerium(IV) complexes containing terminal halide ligands include $CeF[N(SiMe_3)_2]_3$ (**2-F**), recently reported by us,[7] and just two examples of bromide and iodide complexes.[3,8,9] It is therefore desirable to pursue new cerium(IV) halide complexes to expand the chemistry of this unusual oxidation state, identify new starting materials for cerium(IV) chemistry, and demonstrate the physicochemical consequences of systematic ligand variation on the electronic structures in a conserved framework.

The bis(trimethylsilyl)amide ligand (Figure 1) has been well explored in lanthanide coordination chemistry.[10−14] The high degree of steric bulk it confers to lanthanide complexes enables formation of well-defined, low-coordinate monometallic compounds.[15] The synthesis of cerium(IV) silylamide molecular complexes through one-electron oxidation reactions has been shown to be dependent on the choice of oxidant and reaction conditions.[3−5,8,9,16−19] Reported access to cerium(IV) complexes of the bis(trimethylsilyl)amide ligand included oxidation of $Ce[N(SiMe_3)_2]_3$ (**1**) to yield $CeX[N(SiMe_3)_2]_3$ (X = F^-, Cl^-, Br^-)[2,3,5,7] as well as dimeric bridging oxo, peroxo, and diolate complexes.[20,21] In contrast, in the more sterically open silyl-substituted tripodal tris(2-aminoethyl)amine (tren) framework, $[N(CH_2CH_2N(SiMe_2{}^tBu))_3]^{3-}$ (NN'_3), one-electron oxidation of the trivalent precursor with molecular halogens yielded the tetravalent complex $CeI(NN'_3)$ and the mixed-valent dimers $\{Ce(NN'_3)\}_2(\mu\text{-X})$ (X = Cl^-, Br^-).[9] In the related bis(dimethylsilyl)amide ligand framework, halide functionalization was prohibited by ligand redistribution because of reduced steric bulk. Oxidation of the cerium(III) precursor $Ce[N(SiHMe_2)_2]_3(THF)_2$ (THF = tetrahydrofuran) with Ph_3CCl led to isolation of the homoleptic complex $Ce[N(SiHMe_2)_2]_4$ through ligand redistribution.[22] Similarly, the homoleptic cerium(IV) compound $Ce(NCy_2)_4$ was isolated by oxidation of $Ce(NCy_2)_3(THF)$ or $Ce(NCy_2)_2(\mu\text{-}NCy_2)_2Li(THF)$ with O_2.[23]

Having recently reported the synthesis and characterization of the first molecular cerium(IV) fluoride complex **2-F** from one-electron oxidation of **1** concomitant with fluoride abstraction from a PF_6^- or BF_4^- anion[7] and drawing inspiration from the seminal work of Lappert and co-workers,[2,3] we sought to extend the chemistry of this archetypal framework for lanthanide chemistry. In this report, we describe new routes to

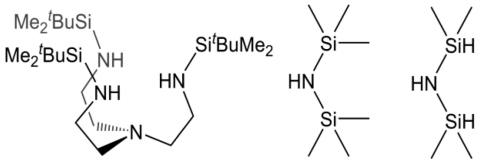

Figure 1. Silylamine ligands used in molecular cerium(IV) chemistry. From left to right, silyl-substituted tris(2-aminoethyl)amine, bis(trimethylsilyl)amine, and bis(dimethylsilyl)amine.

Received: April 25, 2014
Published: May 29, 2014

   dx.doi.org/10.1021/ic500969r | Inorg. Chem. 2014, 53, 6338−6345

the previously reported compounds $CeCl[N(SiMe_3)_2]_3$ and $CeBr[N(SiMe_3)_2]_3$ as well as the synthesis of the new iodide congener $CeI[N(SiMe_3)_2]_3$. The compounds were synthesized by halogen-exchange reactions using trimethylsilyl halide reagents, a new method in cerium(IV) chemistry. We also used the compounds to synthesize pseudohalide cerium(IV) coordination compounds in the bis(trimethylsilyl)amide ancillary ligand environment.

Previous work by our group and others has shown that the ligand environment about a cerium(IV) ion can significantly affect its electrochemical redox potentials and UV−visible electronic transitions.[7,8,19,24−31] Several studies have evaluated the physical properties of the cerium(IV) ion in the bis(trimethylsilyl)amide ligand environment and have shown that these complexes function as mild-to-weak reductants, and exhibit intense ligand-to-metal charge-transfer (LMCT) transitions in the visible range.[7,19,32] With the newly synthesized series of halide and pseudohalide cerium(IV) silylamide compounds in hand, we completed electrochemical, spectroscopic, and computational analyses to describe the effects of halide and pseudohalide coordination to the cerium(IV) center.

RESULTS AND DISCUSSION

Synthesis and Structural Characterization. As we recently reported, the trivalent complex **1** undergoes one-electron oxidation reactions when presented with Ph_3CBF_4, Ph_3CPF_6, $FcBF_4$, or $FcPF_6$, resulting in isolation of the tetravalent complex **2-F**.[7] Taking advantage of Si−F bond formation as a strong thermodynamic driving force, compound **2-F** was reacted with Me_3SiX (X = Cl^-, Br^-, I^-), resulting in conversion to $CeX[N(SiMe_3)_2]_3$ [X = Cl^- (**2-Cl**), Br^- (**2-Br**), I^- (**2-I**)] and Me_3SiF (Scheme 1) in 27−47% isolated yields

Scheme 1. Syntheses of Compounds 2-Cl, 2-Br, and 2-I

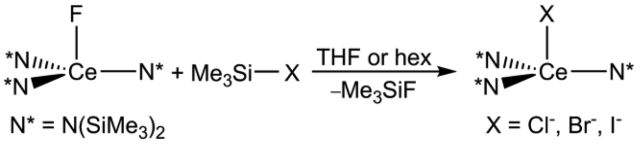

following crystallization from concentrated hexanes solutions at −35 °C. Compound **2-I** was stable in the solid state upon storage at −35 °C and decomposed to an unidentified white solid upon prolonged storage at room temperature. In solution, **2-I** was stable in hexanes and benzene-d_6 but decomposed to **1** upon dissolution in THF.

All of the compounds crystallized solvent-free from hexanes. Full X-ray crystallographic analysis was performed on the previously unreported complex **2-I** and compared to previous studies that evaluated the solid-state structures of **2-F**, **2-Cl**, and **2-Br**.[2,3,7] The structure of **2-I** is depicted in Figure 2, and the crystallographically determined structural parameters for compounds **2-F**, **2-Cl**, **2-Br**, and **2-I** are provided in Table 1.

Compounds **2-Cl**, **2-Br**, and **2-I** crystallized in the rhombohedral *R*3*c* space group with crystallographically imposed C_3 symmetry axes along the Ce−X bond vectors.[2,3] Compound **2-F** crystallized in the monoclinic *P*21/*c* space group with two molecules in the asymmetric unit and displayed approximate C_3 symmetry along the Ce−F bond vectors.[7] The Ce−N bond distances present in compounds **2-Cl**, **2-Br**, and **2-I** were equivalent within experimental error and were intermediate to the range of Ce−N bond distances in

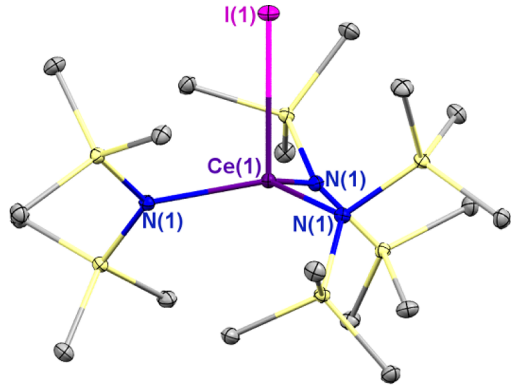

Figure 2. 30% probability thermal ellipsoid plot of compound **2-I**. Hydrogen atoms have been omitted for clarity. Selected bond distances (Å): Ce(1)−N(1) 2.2153(9), Ce(1)−I(1) 2.9980(2).

Table 1. Comparison of Bonding Metrics from the Crystallographically Determined Structures of 2-F, 2-Cl, 2-Br, and 2-I

complex	M−N* (Å)[a]	M−X (Å)	M−N^*_3 displacement (Å)
2-F[b]	2.201(10)−2.254(9)	2.065(6), 2.065(7)	0.166(5), 0.197(5)
2-Cl[c]	2.217(3)	2.597(2)	0.365(3)
2-Br[c]	2.219(7)	2.7662(17)	0.373(9)
2-I	2.2153(9)	2.9980(2)	0.3539(10)

[a]N* = $-N(SiMe_3)_2$. [b]Data reported in ref 7. [c]Data reported in ref 2.

compound **2-F**. As expected, the Ce−X bonds lengthened with coordination of the larger heteroatoms. As a result of the interactions between the coordinated halide ligand and the bulky bis(trimethylsilyl)amide ligands, the compounds showed increasing pyramidalization with the size of the halide ligand (**2-F** < **2-Cl** < **2-Br**), as evidenced by the increased displacement of the cerium ion from the plane formed by the amide nitrogen atoms ($M-N^*_3$ displacement; Table 1). Compound **2-I** showed an exception to this trend and was less pyramidalized than **2-Cl** and **2-Br** despite the large size of the iodide ligand, which evidently did not perturb the geometry of the complex as a result of the long Ce−I bond distance [2.9980(2) Å]. However, the Ce−I bond distance in **2-I** was shorter than the reported Ce−I bond distances in molecular cerium(IV) complexes of 3.1284(6) Å in $CeI(NN'_3)$ and 3.1414(11) Å in $[Li_3(DMEDA)_3][CeI(BINOLate)_3]$.[8,9]

Spectroscopic Characterization. NMR analysis of compounds **2-F**, **2-Cl**, **2-Br**, and **2-I** in benzene-d_6 showed sharp spectral features and chemical shifts consistent with the formally diamagnetic nature of the complexes. The ^{1}H NMR shifts ranged from 0.39 to 0.50 ppm and trended according to the electron-rich nature of the halide (**2-F** < **2-Cl** < **2-Br** < **2-I**). The ^{13}C NMR shifts ranged from 4.75 to 6.43 ppm and displayed a similar trend.

In the IR spectra, compounds **2-F**, **2-Cl**, **2-Br**, and **2-I** showed very similar features in the fingerprint region corresponding to vibrations of the silylamide ligands. The Ce−X stretch was observed experimentally only in the case of **2-F** (at 493 cm^{-1}).[7] The remaining Ce−X stretches were beyond the low-energy limit of the spectrometer, consistent with the computationally predicted vibrational spectra (*vide infra*).

dx.doi.org/10.1021/ic500969r | Inorg. Chem. 2014, 53, 6338−6345

The electronic absorption spectra of **2-F**, **2-Cl**, **2-Br**, and **2-I** collected in hexanes revealed broad transitions in the UV–visible region (Figure 3). These features were assigned as

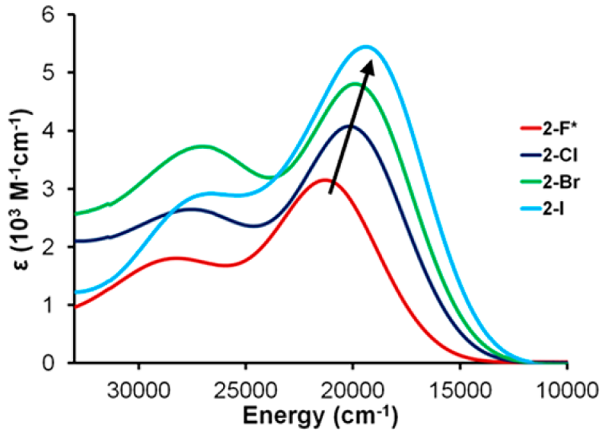

Figure 3. Electronic absorption spectra of **2-F**, **2-Cl**, **2-Br**, and **2-I**, collected in hexanes (* = ×0.5). The arrow indicates the shift in the LMCT energies with increasing halide size.

LMCT transitions, which were characteristic of cerium(IV) coordination compounds.[24,30,31,33] Two prominent features centered at ∼20000 and ∼27000 cm^{-1} were observed in the spectra of **2-F**, **2-Cl**, **2-Br**, and **2-I**. Considering that reported halide-to-cerium(IV) charge-transfer transitions occur in the UV spectral region,[34] the features in the visible portion of the spectra of **2-F**, **2-Cl**, **2-Br**, and **2-I** were tentatively assigned as silylamide-to-cerium(IV) charge-transfer transitions. In the spectra of **2-F**, **2-Cl**, **2-Br**, and **2-I**, the higher-energy features varied by 2204 cm^{-1} and the low-energy features varied by 2603 cm^{-1} (Table 2). The variability of these features indicated

Table 2. LMCT Transition Energies and Molar Absorptivities from the Electronic Absorption Spectra of 2-F, 2-Cl, 2-Br, and 2-I

complex	E (cm^{-1})/ε (M^{-1} cm^{-1})	
2-F	21100/5930	28102/2890
2-Cl	19880/3830	27460/2520
2-Br	19147/4390	25499/3090
2-I	18896/4700	26191/3290

that the identity of the halide ligand impacted the interaction of the cerium ion with its ligand environment. Higher-energy transitions were observed in the spectra of compounds containing the smaller halide ligands, indicating that coordination of the small, electron-rich halides to the cerium center stabilized the ground electronic state of the complex, resulting in an increased energy difference between the electronic states involved in the LMCT transitions.

Electrochemical Characterization. Electrochemical analysis was undertaken in order to describe the effect of the ligand environment on the thermodynamic stability of the cerium(IV) cation. Data were collected in THF with 0.1 M [^{n}Pr$_4$N][BAr$^F_4$]; however, data for compound **2-I** were not obtainable because the compound was unstable under the experimental conditions. Comparing the cyclic voltammogram of **1** to those of the halide-functionalized products demonstrated that the halide ligands stabilized the cerium(IV) center, as reflected in the shift of the $Ce^{III/IV}$ couple to more reducing potentials (Figure 4).

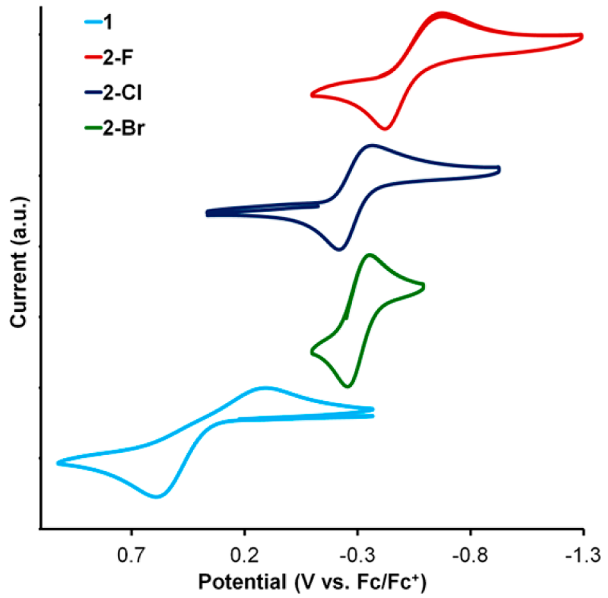

Figure 4. Isolated $Ce^{III/IV}$ redox couples in the cyclic voltammograms of **1**, **2-F**, **2-Cl**, and **2-Br** collected in THF with 0.1 M [^{n}Pr$_4$N][BAr$^F_4$]. [analyte] = ca. 1 mM; ν = 0.05 V s^{-1}.

Compound **2-F** was stabilized by 0.25 V compared to **2-Cl** and **2-Br**, which were observed at comparable potentials of −0.30 and −0.31 V, respectively (Table 3). As shown in Figure 4, the

Table 3. Electrochemical Data for Compounds 1, 2-F, 2-Cl, and 2-Br Collected in THF with 0.1 M [^{n}Pr$_4$N][BAr$^F_4$] ([analyte] = ca. 1 mM; ν = 0.05 V s^{-1})

complex	$E_{1/2}$ (V vs Fc/Fc⁺)	ΔE (V)
1[a]	+0.35	0.64
2-F[a]	−0.56	0.26
2-Cl[b]	−0.30	0.15
2-Br	−0.31	0.08

[a]Data reported in ref 7. [b]Data reported in ref 19.

compounds containing the larger halide ligands resulted in more reversible electrochemical features. The steric demand of the complexes containing large halide ligands (**2-Br** > **2-Cl** > **2-F**) evidently reduced the reorganization energy and led to diminished overpotentials.[18,19,32]

Computational Analysis. Electronic structure calculations of compounds **2-F**, **2-Cl**, **2-Br**, and **2-I** were performed using *Gaussian '09* at the B3LYP level of theory in order to describe the nature of metal–ligand bonding in the complexes. The geometry-optimized gas-phase structures were found to be in excellent agreement with the crystallographically determined bond lengths and bond angles. In each complex, the lowest unoccupied LUMO–LUMO+6 molecular orbitals were primarily nonbonding 4f orbitals localized on the cerium atom. Figure 5 shows the calculated electronic manifold for each complex and depictions of molecular orbitals that included metal–ligand orbital overlap.

The silylamide ligands in compounds **2-F**, **2-Cl**, **2-Br**, and **2-I** interacted with the cerium cation through both weak σ and π donation. The molecular orbitals involved in electron donation through Ce–N σ and π interactions are shown in the topmost orbitals depicted for each complex in Figure 5. The bonding interactions between the cerium ion and the halide ligands in

dx.doi.org/10.1021/ic500969r | Inorg. Chem. 2014, 53, 6338–6345

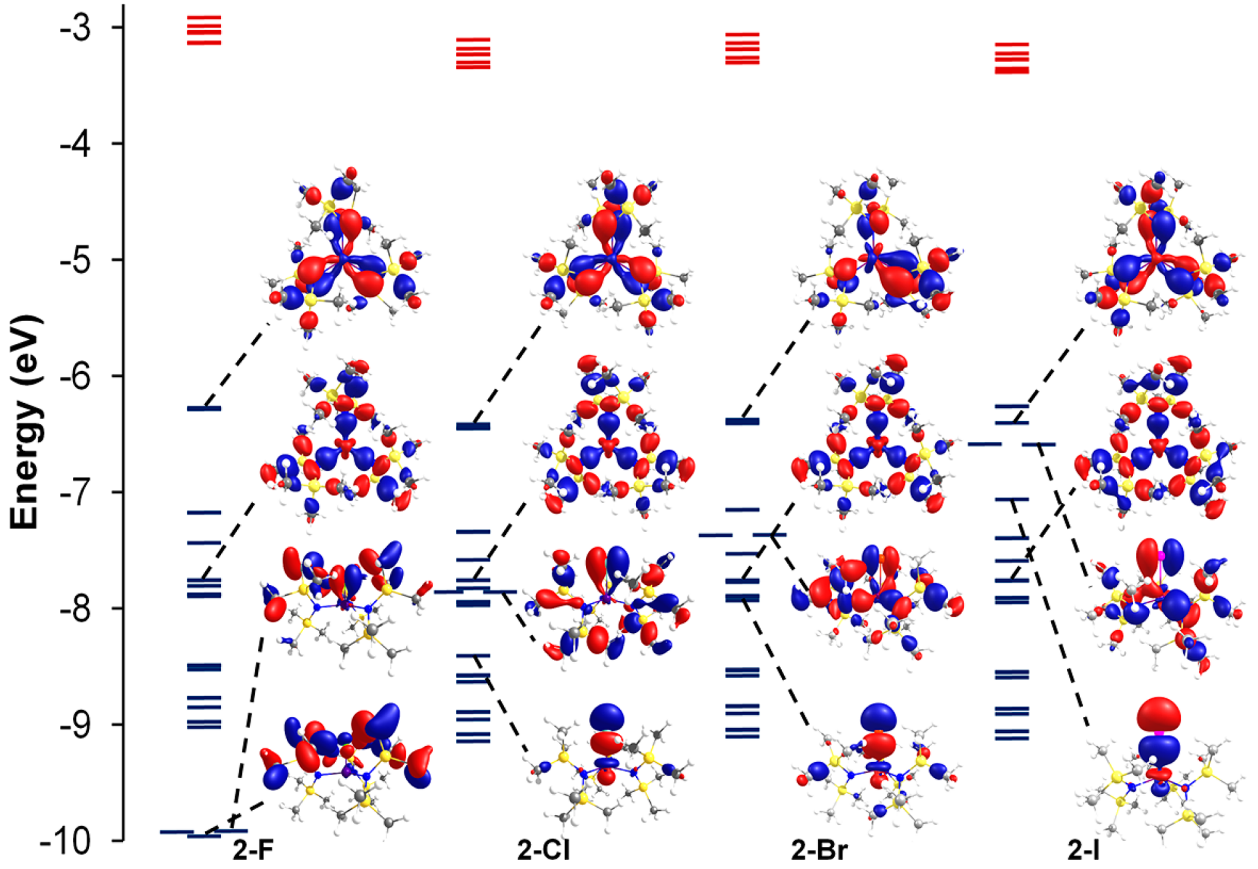

Figure 5. Normalized, computationally determined valence orbital diagrams of **2-F**, **2-Cl**, **2-Br**, and **2-I**. Occupied molecular orbitals are shown in blue, and unoccupied molecular orbitals are shown in red. The molecular orbitals with Ce–X (X = F^-, Cl^-, Br^-, I^-) and Ce–N interactions in the σ and π orientations are shown. From top to bottom, Ce–N π, Ce–N σ, Ce–X π, and Ce–X σ interactions.

compounds **2-F**, **2-Cl**, **2-Br**, and **2-I** were largely ionic in all cases, but molecular orbitals with overlap of the atomic orbitals in both the σ and π orientations were observed. These molecular orbitals are depicted in the bottommost orbitals represented for each compound in Figure 5. The metal–halide bonding interactions in the σ orientation showed increased overlap in compounds containing the heavier halides because of contributions from more diffuse valence atomic orbitals. In contrast, the metal–halide interactions in the π orientation observed in **2-F** and **2-Cl** were minimized in the compounds containing the heavier halide ligands.

Using natural population analysis, natural charges of the cerium and halide atoms and the Ce–X Mayer bond orders were calculated in order to describe the ionicity of the metal–halide bonds in compounds **2-F**, **2-Cl**, **2-Br**, and **2-I** (Table 4). These metrics indicated a slight decrease in the ionicity of the metal–halide bonds when the cerium ion interacted with the heavier halide ions. The observed decrease in the natural charges of the amide nitrogen atoms in complexes containing heavier halides indicated that the identity of the halide impacted the interaction between the cerium and amide ligands, consistent with spectroscopic observations.

Table 4. Natural Charges and Mayer Bond Orders Calculated for 2-F, 2-Cl, 2-Br, and 2-I

complex	q_{Ce}	q_X	$q_{N\ (avg.)}$	MBO_{Ce-X}
2-F	2.081	−0.540	−1.649	0.853
2-Cl	1.902	−0.460	−1.628	1.028
2-Br	1.859	−0.410	−1.626	0.951
2-I	1.840	−0.421	−1.622	1.064

Synthesis and Characterization of Pseudohalide Compounds. In an attempt to extend this series of compounds to include the azide congener $Ce(N_3)[N(SiMe_3)_2]_3$, **2-F** was reacted with Me_3SiN_3 in THF at room temperature, followed by crystallization from a cold hexanes solution. As seen in Scheme 2, this route did lead to anion exchange, forming the dimeric compound $\{Ce[N(SiMe_3)_2]_3(\mu\text{-}N_3)Ce[N(SiMe_3)_2]_3(N_3)\}$ (**2-N_3**). The pseudohalide anion NCS^- coordinated the cerium(IV) ion through a distinct reaction pathway; the reaction of **2-Cl** with NaSCN resulted in metathesis and isolation of $Ce(NCS)[N(SiMe_3)_2]_3$ (**2-NCS**) following workup from hexanes (Scheme 2).

Scheme 2. Synthesis of Compounds 2-N_3 and 2-NCS

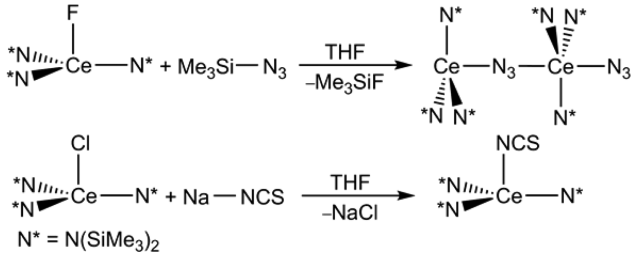

Crystallographic analysis of compound **2-N_3** revealed its dimeric structure with two cerium tris(amide) fragments

dx.doi.org/10.1021/ic500969r | Inorg. Chem. 2014, 53, 6338–6345

bridged by an azide anion in an end-to-end coordination mode and containing a second terminal azide ligand (Figure 6).

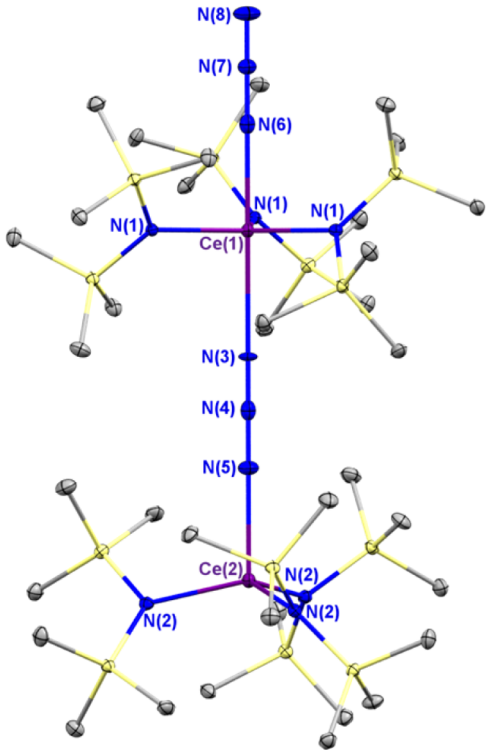

Figure 6. 30% probability thermal ellipsoid plot of compound **2-N$_3$**. Hydrogen atoms have been removed for clarity Selected bond lengths (Å): Ce(1)−N(1) 2.2362(18), Ce(2)−N(2) 2.2000(18), Ce(1)−N(6) 2.250(4), Ce(2)−N(5) 2.379(4), Ce(1)−N(3) 2.665(4). Selected bond angles (deg): N(7)−N(6)−Ce(1) 180.000(1), Ce(1)−N(3)−N(4) 180.000(1), N(4)−N(5)−Ce(2) 180.000(1).

Compound **2-N$_3$** crystallized in the rhombohedral *R*3 space group and displayed crystallographically imposed C_3 symmetry along the axis containing both cerium ions and all three nitrogen atoms of each azide ligand. The cerium−amide bond distances of 2.2362(18) and 2.2000(18) Å were equivalent within experimental error to the cerium−amide distances present in **2-F**, **2-Cl**, **2-Br**, and **2-I**. The molecular unit included a linear axis along the cerium azide axis, with bond angles ranging from 180.000(1) to 180.000(5)°. Of the two cerium(IV) azide complexes that have been previously reported in the literature, both contained bent Ce−N−N bond angles ranging from 133.4(2) to 144.8(3)°.[8,35] Compound **2-N$_3$** packed with all of the cerium−azide bond vectors aligned along the crystallographic *c* axis. The solid-state packing of **2-N$_3$** revealed a weak intermolecular contact between the outermost nitrogen in the terminal azide ligand and the four-coordinate cerium ion at a distance of 4.806(8) Å (Figure S1 in the Supporting Information, SI).

The solid-state structure of monomeric compound **2-NCS** is shown in Figure 7. Compound **2-NCS** crystallized in the monoclinic *P*21/*c* space group and displayed approximate C_3 symmetry along the Ce(1)−N(4) bond vector. The cerium−amide bond distances ranged from 2.2020(14) to 2.2225(14) Å and were comparable within experimental error to the cerium−amide distances present in **2-F**, **2-Cl**, **2-Br**, and **2-I** (Table 5). The cerium ion in the solid-state structure of **2-NCS** was displaced from the plane formed by the amide nitrogen atoms

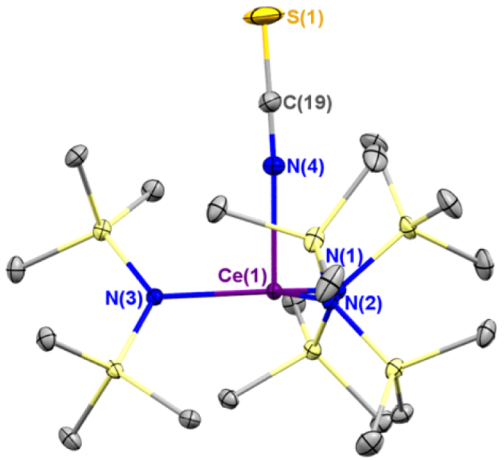

Figure 7. 30% probability thermal ellipsoid plot of compound **2-NCS**. Hydrogen atoms have been removed for clarity. Selected bond lengths (Å): Ce(1)−N(1) 2.2141(14), Ce(1)−N(2) 2.2225(14), Ce(1)−N(3) 2.2020(14), Ce(1)−N(4) 2.3066(15). Selected bond angles (deg): S(1)−C(19)−N(4) 178.9(2), C(19)−N(4)−Ce(1) 175.44(16).

Table 5. Comparison of Bonding Metrics from the Crystallographically Determined Structures of 2-N$_3$ and 2-NCS

complex	M−N* (Å)[a]	M−X (Å)	M−N*$_3$ (Å)[a]
2-N$_3$	2.2362(18), 2.2000(18)	2.250(4), 2.379(4)	0.1017(19), 0.4920(19)
2-NCS	2.2020(14)−2.2225(14)	2.3066(15)	0.0855(8)

[a]N* = −N(SiMe$_3$)$_2$.

by only 0.0855(8) Å. The cerium ion was bonded to the NCS$^-$ ligand in an approximately linear orientation; the Ce(1)−N(4)−C(19) angle was 175.44(16)°, and the N(4)−C(19)−S(1) angle was 178.9(2)°. A single example of a cerium(IV) isothiocyanate was previously reported by our group, which displayed bent Ce−N−C bond angles [154.0° and 154.6(3)°] and longer Ce−N bond distances [2.414(4) and 2.421(3) Å] than that observed in **2-NCS** [2.3055(15) Å].[8]

In the IR region of the absorption spectra, compounds **2-N$_3$** and **2-NCS** showed similar features in the fingerprint region corresponding to vibrations of the silylamide ligand environment. Compound **2-N$_3$** showed two azide asymmetric stretching modes at 2103 and 2085 cm^{-1}. The presence of both bands indicated that the dimer was intact in the Nujol mull, and the similar energies of these features indicated that the neutral donation of the bridging azide ligand to the planarized cerium(IV) ion had only a marginal effect on the electronics of the bridging azide compared to the terminal azide. Density functional theory (DFT) calculations of monomeric Ce(N$_3$)[N(SiMe$_3$)$_2$]$_3$ predicted an asymmetric stretch at 2236 cm^{-1}. The symmetric azide stretching and azide bending modes were unobserved in the experimentally determined spectrum because they coincided with the Nujol and silylamide vibrations. Compound **2-NCS** showed features at 2009 and 490 cm^{-1} corresponding to the stretching and bending modes of the NCS$^-$ ligand, respectively, which were computationally determined at 2060 and 492 cm^{-1}.

The solution structure of **2-N$_3$** was not well-defined. Following isolation of **2-N$_3$**, dissolution in benzene-d_6 or pyridine-d_5 resulted in the loss of HN(SiMe$_3$)$_2$, as identified by

dx.doi.org/10.1021/ic500969r | Inorg. Chem. 2014, 53, 6338−6345

^{1}H NMR analysis. Considering the ambiguous identity of the compound following this decomposition, further analysis of the solution-state properties of **2-N$_3$** was not pursued.

^{1}H and ^{13}C NMR analysis of monomeric **2-NCS** in benzene-d_6 revealed sharp peaks at 0.36 and 4.90 ppm, respectively. As expected in comparison to the absorption spectra of **2-F**, **2-Cl**, **2-Br**, and **2-I**, the electronic absorption spectrum of **2-NCS** collected in hexanes revealed two broad features in the visible region at energies of 20046 cm^{-1} (ε = 7539 M^{-1} cm^{-1}) and 25726 cm^{-1} (ε = 5244 M^{-1} cm^{-1}), assigned as LMCT transitions arising from donation of electron density from the silylamide ligands to the cerium cation. Electrochemical analysis of **2-NCS** performed in THF with 0.1 M [^{n}Pr$_4$N][BAr$^F_4$] showed a reversible metal-based redox event at $E_{1/2}$ = −0.29 V vs Fc/Fc$^+$ (Figure 8). The comparable reduction potentials of

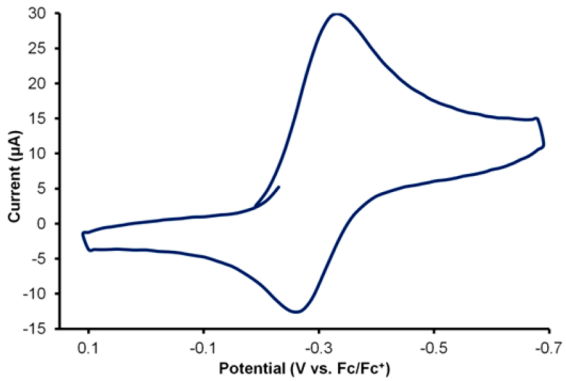

Figure 8. Isolated Ce$^{III/IV}$ redox couple in the cyclic voltammogram of **2-NCS** collected in THF with 0.1 M [^{n}Pr$_4$N][BAr$^F_4$]. [analyte] = ca. 1 mM; ν = 1.0 V s^{-1}. $E_{1/2}$ = −0.29 V vs Fc/Fc$^+$; ΔE = 0.08 V.

the cerium(IV) chloride, bromide, and isothiocyanate compounds were consistent with a family of cerium(IV) tris(BINOLate) compounds recently reported by our group.[8]

CONCLUSIONS

Taking advantage of the reactivity of **2-F**, we synthesized CeX[N(SiMe$_3$)$_2$]$_3$ (X = Cl$^-$, Br$^-$) through new synthetic routes and isolated CeI[N(SiMe$_3$)$_2$]$_3$ for the first time. This series of complexes represents the first complete family of cerium(IV) halide compounds in a concerted ligand framework. We also extended this series to include complexes of pseudohalide ions and isolated rare examples of cerium(IV) coordination compounds containing terminal N_3^- and NCS^- ligands. Spectroscopic analysis demonstrated that the complexes showed amide-based LMCT transitions in the visible region of the spectrum and that the energies of these transitions varied depending on the identity of the halide or pseudohalide ligand. Electrochemical analysis of CeX[N(SiMe$_3$)$_2$]$_3$ (X = F$^-$, Cl$^-$, Br$^-$, NCS$^-$) indicated that stabilization of the cerium(IV) ion depended on the identity of the halide or pseudohalide ligand and that the electron-rich fluoride ligand stabilized the cerium(IV) ion more than the other ligands.

EXPERIMENTAL SECTION

General Methods. All reactions and manipulations were performed under an inert atmosphere (N_2) using standard Schlenk techniques or in a Vacuum Atmospheres, Inc., Nexus II drybox equipped with a molecular sieve 13X/Q5 Cu-0226S catalyst purifier system. Glassware was oven-dried for 3 h at 150 °C prior to use. ^{1}H and ^{13}C NMR spectra were obtained on a Bruker DMX-300 Fourier transform NMR spectrometer at 300 and 91 MHz. Chemical shifts were recorded in units of parts per million (ppm) referenced to residual solvent peaks (^{1}H NMR) or characteristic solvent peaks (^{13}C{^{1}H} NMR). The UV−visible absorption spectra were obtained from 1000−300 nm using a PerkinElmer 950 UV−visible/NIR spectrophotometer, and all samples were prepared under an N_2 environment. Screw-cap quartz cells (1 mm path length) were used with a blank measured before each run. Deconvolution of the UV−visible spectra was performed using fityk.[36] Elemental analyses were performed at the University of California, Berkeley, Microanalytical Facility using a PerkinElmer series II 2400 CHNS analyzer.

Electrochemistry. Cyclic voltammetry (CV) experiments were performed using a CH Instruments 620D Electrochemical Analyzer/Workstation, and the data were processed using *CHI*, version 9.24, software. All experiments were performed in an N_2 atmosphere drybox using electrochemical cells that consisted of a 4 mL vial, a glassy carbon (2 mm diameter) working electrode, a platinum wire counter electrode, and a silver wire plated with AgCl as a quasi-reference electrode. The working electrode surfaces were polished prior to each set of experiments. Potentials were reported versus ferrocene, which was added as an internal standard for calibration at the end of each run. Solutions employed during CV studies were ∼1 mM analyte and 100 mM [^{n}Pr$_4$N][B(3,5-(CF$_3$)$_2$-C$_6$H$_3$)$_4$] ([^{n}Pr$_4$N][BAr$^F_4$]). All data were collected in a positive-feedback IR compensation mode. The solution cell resistances were measured prior to each run to ensure resistances ≤∼500 Ω.

X-ray Crystallography. X-ray intensity data were collected on a Bruker APEX II CCD area detector employing graphite-monochromated Mo Kα radiation (λ = 0.71073 Å) at a temperature of 100(1) K. Preliminary indexing was performed from a series of 36 0.5° rotation frames with exposures of 10 s. Following full data collection, rotation frames were integrated using *SAINT*,[37] producing a listing of unaveraged F^2 and $\sigma(F^2)$ values that were then passed to the *SHELXTL* program package for further processing and structure solution.[38] The intensity data were corrected for Lorentz and polarization effects and for absorption using *SADABS*.[39] The structures were solved by direct methods (*SHELXS-97*).[40] Refinement was by full-matrix least squares based on F^2 using *SHELXL-97*.[40] All reflections were used during refinement. Non-hydrogen atoms were refined anisotropically, and hydrogen atoms were refined using a riding model.

In the structure of **2-N$_3$**, the molecule lay on a crystallographic 3-fold axis (at $^2/_3$, $^1/_3$, z). The rotation axis passed through Ce(1), Ce(2), N(3), N(4), N(5), N(6), N(7), and N(8). During refinement, several atoms went nonpositive definite and R_1 did not refine <12%. Examination of the disagreeable reflections suggested the possibility of twinning (F_o^2 was always greater than F_c^2). ROTAX62 indicated merohedral twinning by 180° rotation about the direct *a* direction. The twinning matrix {1 0 0−1 −1 0 0 0−1} was applied during least-squares refinement. Racemic twinning was also significant. The twinning parameters (including racemic twinning) refined to values of 0.208(4), 0.081(5), and 0.153(4).

Computational Details. *Gaussian '09*, revision A.02, was used in electronic structure calculations.[41] The B3LYP hybrid DFT method was employed with a 28-electron small-core pseudopotential on cerium with published segmented natural orbital basis sets incorporating quasi-relativistic effects[42] and the 6-31G* basis set on all other atoms. Geometry optimizations were carried out starting from the coordinates of the crystal structures. The frequency calculation indicated that the geometry was the minimum (no imaginary frequencies). Molecular orbitals were rendered with the program *Chemcraft*, version 1.6, at an isovalue of 0.03.[43] Natural population analysis was performed using the IOp(6/80=1) keyword in *Gaussian 09*.

Materials. THF, hexanes, and acetonitrile were purchased from Fisher Scientific. These solvents were sparged for 20 min with dry argon and dried using a commercial solvent purification system comprising two columns packed with Q5 reactant and neutral alumina, respectively (for hexanes and acetonitrile), or two columns of neutral alumina (for THF). FcBF$_4$ (Sigma-Aldrich) and Me$_3$SiN$_3$ (Acros

dx.doi.org/10.1021/ic500969r | Inorg. Chem. 2014, 53, 6338−6345

Organics) were purchased and used as received. Me_3SiCl was purchased from Acros Organics and degassed before use. NaSCN was dried at 150 °C overnight before use. Ferrocene (Fc) was purchased from Acros Organics and purified by sublimation before use. Benzene-d_6 was purchased from Cambridge Isotopes and dried over a potassium mirror for 24 h before use. **1**,[15] $[^nPr_4N][BAr^F{}_4]$,[44] Me_3SiBr,[45] and Me_3SiI[45] were prepared according to literature procedures.

*Alternate Synthesis of CeF[N(SiMe$_3$)$_2$]$_3$ (**2-F**).* **2-F** was synthesized as previously reported by oxidation of **1** with Ph_3CBF_4 or by the following method. $FcBF_4$ (0.220 g, 0.806 mmol) was added to a solution of 0.500 g (0.805 mmol) of **1** dissolved in ∼10 mL hexanes, causing a color change to dark red. The reaction mixture was stirred at room temperature for 2 h and then dried under reduced pressure. The reaction mixture was resuspended in ∼5 mL of MeCN, filtered over a medium-porosity fritted filter, washed with ∼3 mL of MeCN, and dried under reduced pressure. The isolated red powder was extracted with ∼10 mL of hexanes, filtered through a Celite-packed filter, and dried under reduced pressure to isolate a pure product as a microcrystalline dark-red solid. Total isolated yield: 0.253 g (0.395 mmol, 49%). ^{1}H NMR (benzene-d_6): δ 0.39 (s, 54H, Si(CH_3)$_3$). ^{13}C{^{1}H} NMR (benzene-d_6): δ 4.75 (Si(CH_3)$_3$).^{19}F NMR (benzene-d_6): δ 312.34 (s, Ce−*F*). Characterization data were consistent with our previous report.[7]

*Synthesis of CeCl[N(SiMe$_3$)$_2$]$_3$ (**2-Cl**).* Me_3SiCl (0.052 g, 0.479 mmol, 6.1 equiv) was dissolved in ∼2 mL of THF and added to a solution of **2-F** (0.050 g, 0.078 mmol) in ∼3 mL of THF. The mixture was stirred for 4.5 h at room temperature. Volatiles were removed under reduced pressure. The dark-purple powder was redissolved in ∼7 mL of hexanes, filtered through a Celite-packed filter, and chilled at −35 °C to induce crystallization. The mother liquor was removed by decantation, and the crystals were dried under reduced pressure, giving the product as dark-purple crystals. Yield: 0.024 g (0.037 mmol, 47%). ^{1}H NMR (benzene-d_6): δ 0.43 (s, 54H, Si(CH_3)$_3$). ^{13}C{^{1}H} NMR (benzene-d_6): δ 5.40 (Si(CH_3)$_3$). Characterization data were consistent with previous reports.[2,3]

*Synthesis of CeBr[N(SiMe$_3$)$_2$]$_3$ (**2-Br**).* **2-F** (0.050 g, 0.078 mmol) was dissolved ∼3 mL of THF. Me_3SiBr (0.483 mmol, 6 equiv) was added in ∼2 mL of THF, and the reaction was stirred at room temperature for 4.5 h. Volatiles were removed under reduced pressure. The resultant dark-purple powder was dissolved in ∼7 mL of hexanes and chilled at −35 °C to induce crystallization. The mother liquor was removed by decantation, and the crystals were washed one time with 1 mL of hexanes and dried under reduced pressure, giving the product as dark-purple crystals. Yield: 0.015 g (0.021 mmol, 27%). ^{1}H NMR (benzene-d_6): δ 0.46 (s, 54H, Si(CH_3)$_3$). ^{13}C{^{1}H} NMR (benzene-d_6): δ 5.76 (Si(CH_3)$_3$). Characterization data were consistent with previous reports.[3]

*Synthesis of CeI[N(SiMe$_3$)$_2$]$_3$ (**2-I**).* **2-F** (0.051 g, 0.080 mmol) was dissolved in ∼5 mL of hexanes. Me_3SiI (0.098 mmol, 12 equiv) was added in ∼3 mL hexanes, and the reaction was stirred for 6 h at room temperature. Volatiles were stripped from the dark-purple solution. The resultant dark-purple solid was dissolved in ∼15 mL of hexanes and chilled at −35 °C to induce crystallization. The mother liquor was removed by decantation, and the crystals were washed one time with 1 mL of hexanes and dried under reduced pressure, giving the product as dark-purple crystals. Yield: 0.026 g (0.037 mmol, 43%). Anal. Calcd for $CeC_{18}H_{54}N_3Si_6I$: C, 28.89; H, 7.28; N, 5.62. Found: C, 29.14; H, 7.16; N, 5.53. ^{1}H NMR (benzene-d_6): δ 0.50 (s, 54H, Si(CH_3)$_3$). ^{13}C{^{1}H} NMR (benzene-d_6): δ 6.43 (Si(CH_3)$_3$).

*Synthesis of {Ce[N(SiMe$_3$)$_2$]$_3$(μ-N$_3$)Ce[N(SiMe$_3$)$_2$]$_3$(N$_3$)} (**2-N$_3$**).* **2-F** (0.100 g, 0.156 mmol) was dissolved in ∼5 mL of THF. Me_3SiN_3 (0.095 g, 0.824 mmol, 5.3 equiv) was added and stirred overnight at room temperature. Volatiles were stripped from the resultant dark-red solution. The resulting dark-red solid was dissolved in ∼12 mL of hexanes and chilled at −35 °C to induce crystallization. The mother liquor was removed by decantation and dried under reduced pressure, giving the product as a dark-red powder. Yield: 0.028 g (0.042 mmol, 27%). Anal. Calcd for $Ce_2C_{36}H_{108}N_9Si_{12}$: C, 32.59; H, 8.21; N, 12.67. Found: C, 33.04; H, 8.25; N, 12.78.

*Synthesis of Ce(NCS)[N(SiMe$_3$)$_2$]$_3$ (**2-NCS**).* **2-Cl** (0.376 g, 0.573 mmol) was dissolved in ∼10 mL of THF. NaSCN (0.065 g, 0.802 mmol, 1.4 equiv) was added, causing a color change from dark purple to dark red. The mixture was stirred at room temperature overnight. Volatiles were removed under reduced pressure, and the product was extracted with ∼30 mL of hexanes and filtered through a Celite-packed filter to remove the NaCl byproduct. The solution was concentrated to a volume of ∼1 mL and chilled at −35 °C to induce crystallization. The mother liquor was removed by decantation, and the crystals were dried under reduced pressure, giving the product as dark-red crystals. Yield: 0.154 g (0.227 mmol, 40%). Anal. Calcd for $CeC_{19}H_{54}N_4Si_6S$: C, 33.59; H, 8.01; N, 8.25. Found: C, 33.46; H, 7.88; N, 7.99. ^{1}H NMR (benzene-d_6): δ 0.36 (s, 54H, Si(CH_3)$_3$). ^{13}C{^{1}H} NMR (benzene-d_6): δ 4.91 (Si(CH_3)$_3$).

■ ASSOCIATED CONTENT

Ⓢ Supporting Information

X-ray crystallographic data in CIF format, NMR data, crystallographic data, electronic absorption data, IR spectroscopy data, cyclic voltammograms, and DFT results. This material is available free of charge via the Internet at http://pubs.acs.org.

■ AUTHOR INFORMATION

Corresponding Author

*E-mail: schelter@sas.upenn.edu.

Notes

The authors declare no competing financial interest.

■ ACKNOWLEDGMENTS

The authors gratefully acknowledge the Chemical Sciences, Geosciences, and Biosciences Division, Office of Basic Energy Sciences, Early Career Research Program of the U.S. Department of Energy (Award DE-SC0006518). We also thank the University of Pennsylvania and the Research Corporation for Science Advancement (Cottrell Scholar Award to E.J.S.) for financial support and the NSF for support of the X-ray diffractometer (Grant CHE-0840438) and computational resources (Grant 0131132).

■ REFERENCES

(1) Rogers, E.; Dorenbos, P.; van der Kolk, E. *New J. Phys.* **2011**, *13*, 093038/1−093038/32.
(2) Eisenstein, O.; Hitchcock, P. B.; Hulkes, A. G.; Lappert, M. F.; Maron, L. *Chem. Commun.* **2001**, 1560−1561.
(3) Hitchcock, P. B.; Hulkes, A. G.; Lappert, M. F. *Inorg. Chem.* **2004**, *43*, 1031−1038.
(4) Dröse, P.; Crozier, A. R.; Lashkari, S.; Gottfriedsen, J.; Blaurock, S.; Hrib, C. G.; Maichle-Mössmer, C.; Schädle, C.; Anwander, R.; Edelmann, F. T. *J. Am. Chem. Soc.* **2010**, *132*, 14046−14047.
(5) Arnold, P. L.; Turner, Z. R.; Kaltsoyannis, N.; Pelekanaki, P.; Bellabarba, R. M.; Tooze, R. P. *Chem.—Eur. J.* **2010**, *16*, 9623−9629.
(6) Wang, G.-C.; Sung, H. H. Y.; Williams, I. D.; Leung, W.-H. *Inorg. Chem.* **2012**, *51*, 3640−3647.
(7) Williams, U. J.; Robinson, J. R.; Lewis, A. J.; Carroll, P. J.; Walsh, P. J.; Schelter, E. J. *Inorg. Chem.* **2014**, *53*, 27−29.
(8) Robinson, J. R.; Gordon, Z.; Booth, C. H.; Carroll, P. J.; Walsh, P. J.; Schelter, E. J. *J. Am. Chem. Soc.* **2013**, *135*, 19016−19024.
(9) Morton, C.; Alcock, N. W.; Lees, M. R.; Munslow, I. J.; Sanders, C. J.; Scott, P. *J. Am. Chem. Soc.* **1999**, *121*, 11255−11256.
(10) Anwander, R. *Top. Curr. Chem.* **1996**, *179*, 33−112.
(11) Lappert, M.; Protchenko, A.; Power, P.; Seeber, A. Amides of the Group 3 and Lanthanide Metals. *Metal Amide Chemistry*; John Wiley & Sons, Ltd.: New York, 2008; pp 79−120.
(12) Dehnicke, K.; Greiner, A. *Angew. Chem., Int. Ed.* **2003**, *42*, 1340−1354.

(13) Roesky, P. W. *Z. Anorg. Allg. Chem.* **2003**, *629*, 1881−1894.
(14) Evans, W. J.; Johnston, M. A.; Clark, R. D.; Anwander, R.; Ziller, J. W. *Polyhedron* **2001**, *20*, 2483−2490.
(15) Bradley, D. C.; Ghotra, J. S.; Hart, F. A. *J. Chem. Soc., Dalton Trans.* **1973**, 1021−1023.
(16) Hitchcock, P. B.; Hulkes, A. G.; Lappert, M. F.; Li, Z. *Dalton Trans.* **2004**, 129−136.
(17) Hitchcock, P. B.; Huang, Q.-G.; Lappert, M. F.; Wei, X.-H. *J. Mater. Chem.* **2004**, *14*, 3266−3273.
(18) Casely, I. J.; Liddle, S. T.; Blake, A. J.; Wilson, C.; Arnold, P. L. *Chem. Commun.* **2007**, 5037−5039.
(19) Robinson, J. R.; Carroll, P. J.; Walsh, P. J.; Schelter, E. J. *Angew. Chem., Int. Ed.* **2012**, *51*, 10159−10163.
(20) Coles, M. P.; Hitchcock, P. B.; Khvostov, A. V.; Lappert, M. F.; Li, Z.; Protchenko, A. V. *Dalton Trans.* **2010**, *39*, 6780−6788.
(21) Werner, D.; Deacon, G. B.; Junk, P. C.; Anwander, R. *Chem.—Eur. J.* **2014**, *20*, 4426−4438.
(22) Crozier, A. R.; Bienfait, A. M.; Maichle-Mossmer, C.; Tornroos, K. W.; Anwander, R. *Chem. Commun.* **2013**, *49*, 87−89.
(23) Hitchcock, P. B.; Lappert, M. F.; Protchenko, A. V. *Chem. Commun.* **2006**, 3546−3548.
(24) Vogler, A.; Kunkely, H. *Inorg. Chim. Acta* **2006**, *359*, 4130−4138.
(25) Robinson, J. R.; Booth, C. H.; Carroll, P. J.; Walsh, P. J.; Schelter, E. J. *Chem.—Eur. J.* **2013**, *19*, 5996−6004.
(26) Mahoney, B. D.; Piro, N. A.; Carroll, P. J.; Schelter, E. J. *Inorg. Chem.* **2013**, *52*, 5970−5977.
(27) Bogart, J. A.; Lewis, A. J.; Medling, S. A.; Piro, N. A.; Carroll, P. J.; Booth, C. H.; Schelter, E. J. *Inorg. Chem.* **2013**, *52*, 11600−11607.
(28) Lee, H. B.; Bogart, J. A.; Carroll, P. J.; Schelter, E. J. *Chem. Commun.* **2014**, DOI: 10.1039/C3CC46486E.
(29) Dorfner, W. L.; Carroll, P. J.; Schelter, E. J. *Dalton Trans.* **2014**, *43*, 6300−6303.
(30) Gregson, M.; Lu, E.; McMaster, J.; Lewis, W.; Blake, A. J.; Liddle, S. T. *Angew. Chem., Int. Ed.* **2013**, *52*, 13016−13019.
(31) Horváth, O.; Stevenson, K. L. *Charge transfer photochemistry of coordination compounds*; VCH Publishers, Inc.: New York, 1993; pp 86−89.
(32) Piro, N. A.; Robinson, J. R.; Walsh, P. J.; Schelter, E. J. *Coord. Chem. Rev.* **2014**, *260*, 21−36.
(33) Ciampolini, M.; Mani, F.; Nardi, N. *J. Chem. Soc., Dalton Trans.* **1977**, 1325−1328.
(34) Ryan, J. L.; Jørgensen, C. K. *J. Phys. Chem.* **1966**, *70*, 2845−2857.
(35) Dröse, P.; Gottfriedsen, J.; Hrib, C. G.; Jones, P. G.; Hilfert, L.; Edelmann, F. T. *Z. Anorg. Allg. Chem.* **2011**, *637*, 369−373.
(36) Wojdyr, M. *J. Appl. Crystallogr.* **2010**, *43*, 1126−1128.
(37) *SAINT*; Bruker AXS, Inc.: Madison, WI, 2009.
(38) *SHELXTL*, Bruker AXS, Inc.: Madison, WI, 2009.
(39) Sheldrick, G. M. *SADABS*; University of Gottingen: Gottingen, Germany, 2007.
(40) Sheldrick, G. *Acta Crystallogr., Sect. A* **2008**, *64*, 112−122.
(41) Frisch, M. J.; Trucks, G. W.; Schlegel, H. B.; Scuseria, G. E.; Robb, M. A.; Cheeseman, J. R.; Scalmani, G.; Barone, V.; Mennucci, B.; Petersson, G. A.; Nakatsuji, H.; Caricato, M.; Li, X.; Hratchian, H. P.; Izmaylov, A. F.; Bloino, J.; Zheng, G.; Sonnenberg, J. L.; Hada, M.; Ehara, M.; Toyota, K.; Fukuda, R.; Hasegawa, J.; Ishida, M.; Nakajima, T.; Honda, Y.; Kitao, O.; Nakai, H.; Vreven, T.; Montgomery, J. A., Jr.; Peralta, J. E.; Ogliaro, F.; Bearpark, M.; Heyd, J. J.; Brothers, E.; Kudin, K. N.; Staroverov, V. N.; Kobayashi, R.; Normand, J.; Raghavachari, K.; Rendell, A.; Burant, J. C.; Iyengar, S. S.; Tomasi, J.; Cossi, M.; Rega, N.; Millam, J. M.; Klene, M.; Knox, J. E.; Cross, J. B.; Bakken, V.; Adamo, C.; Jaramillo, J.; Gomperts, R.; Stratmann, R. E.; Yazyev, O.; Austin, A. J.; Cammi, R.; Pomelli, C.; Ochterski, J. W.; Martin, R. L.; Morokuma, K.; Zakrzewski, V. G.; Voth, G. A.; Salvador, P.; Dannenberg, J. J.; Dapprich, S.; Daniels, A. D.; Farkas, Ö.; Foresman, J. B.; Ortiz, J. V.; Cioslowski, J.; Fox, D. J. *Gaussian 09*, revision A.02; Gaussian, Inc.: Wallingford, CT, 2009.
(42) Dolg, M.; Stoll, H.; Preuss, H. *J. Chem. Phys.* **1989**, *90*, 1730−1734.
(43) Zhurko, G. A.; Zhurko, D. A. http://chemcraftprog.com/.
(44) Thomson, R. K.; Scott, B. L.; Morris, D. E.; Kiplinger, J. L. *C. R. Chim.* **2010**, *13*, 790−802.
(45) Friedrich, E. C.; DeLucca, G. *J. Org. Chem.* **1983**, *48*, 1678−1682.